Journal of Power Sources 196 (2011) 8241–8249

Contents lists available at ScienceDirect

Journal of Power Sources

journal homepage: www.elsevier.com/locate/jpowsour

Fabrication process analysis and experimental verification for aluminum bipolar plates in fuel cells by vacuum die-casting

Chul Kyu Jin[a], Chung Gil Kang[b,*]

[a] Precision Manufacturing System Division, Graduate School, Pusan National University, San 30 Chang Jun-dong, Geum Jung-Gu, Busan 609-735, South Korea
[b] Engineering Research Center for Net Shape and Die Manufacturing, School of Mechanical Engineering, Pusan National University, San 30 Chang Jun-dong, Geum Jung-Gu, Busan 609-735, South Korea

ARTICLE INFO

Article history:
Received 28 March 2011
Received in revised form 23 April 2011
Accepted 27 May 2011
Available online 2 June 2011

Keywords:
Vacuum die casting
Die design
Injection speed
Bipolar plate

ABSTRACT

There are various methods for the fabrication of bipolar plates, but these are still limited to machining and stamping processes. High-pressure die casting (HPDC) is an ideal process for the manufacture of bipolar plates This study aims to investigate the formability of bipolar plates for polymer electrolyte membrane fuel cells (PEMFCs) fabricated by vacuum HPDC of an Al–Mg alloy (ALDC6). The cavity of the mold consisted of a thin-walled plate (200 mm × 200 mm × 0.8 mm) with a layer of serpentine channel (50 mm × 50 mm). The location and direction of the channel in the final mold design was determined by computational simulation (MAGMA soft). In addition, simulation results for different conditions of plunger stroke control were compared to those from actual die-casting experiments. Under a vacuum pressure of 35 kPa and for injection speeds of 0.3 and 2.5 m s^{-1} in the low and high speed regions, respectively, the samples had few casting defects. In addition, the hardness was higher and porosity in microstructure was less than those of the samples made under other injection speed conditions. In case of thin-walled plates, vacuum die casting is beneficial in terms of formability compared to conventional die casting.

1. Introduction

The hydrogen fuel cell is a promising alternative power-generation system for a variety of applications, and its use would reduce the consumption of fossil fuels. Polymer electrolyte membrane fuel cells (PEMFCs) have received considerable attention to replace the internal combustion engine in transportation applications because of their unique properties such as fast start-up, low operation temperature, and high power density, more research is being conducted on their use in the internal combustion engines of vehicles [1].

Among the various components of the fuel cell, the bipolar plates make up about 50% of the stack volume, 60–80% of the stack weight, and 30–50% of the stack fabrication cost. The bipolar plate is a very important component in PEMFC systems. It collects the electrons generated by an electrochemical reaction in the membrane electrode assembly (MEA), uniformly distributes the reactant gases (H_2, O_2) passing through the micro-flow channel, and acts as a structural support for the fuel-cell components [2,3]. The gas flow-field design in a bipolar plate is related to fuel-cell performance, and as such the effective design of the gas flow-field through optimization of the channel dimensions, shape, and configuration is crucial for improving the bipolar plate.

Metallic bipolar plates have advantages over graphite and polymer–carbon composite bipolar plates in terms of their low mass, low-cost stack fabrication, and their high electrical conductivity, in addition to their excellent mechanical properties. However, there are two main drawbacks of metallic bipolar plates. The first is their poor corrosion resistance, which causes MEA poisoning and degradation of the fuel-cell system. The second problem is the lack of manufacturing processes that offer low-cost, high-speed, and precision mass production of the thin metallic plates [4].

In the last few years, several fabrication research of the metallic bipolar plate has been carried out. Lee et al. [5] developed an electrochemical micro-machining (EMM) process for micro-scaled flow channels on metallic bipolar plates, and demonstrated that the EMM process is efficient method for them because the actual fabrication of flow channels on SS316 thin plate takes only 5 min. Hung et al. [6] machined channel with a depth and rib width of 500 μm, and height of 600 μm (aspect ratio of 1.2) in a reaction area 20 mm × 20 mm on 50 mm × 50 mm × 1 mm SUS 316L stainless steel using microelectrical discharge machining milling (micro EDM milling). In addition, they reported that bipolar plate with aspect ratio of 1.2 can promote performance of microfuel cells. Mahabunphachai et al. [7] studied the formability and surface topography issues of metallic bipolar plates fabricated by stamping

* Corresponding author. Tel.: +82 51 510 1455; fax: +82 51 518 1456.
E-mail address: cgkang@pusan.ac.kr (C.G. Kang).

0378-7753/$ – see front matter © 2011 Elsevier B.V. All rights reserved.
doi:10.1016/j.jpowsour.2011.05.073

and hydroforming, and reported that hydroforming was observed to provide bipolar plates with lower dimensional variations than the stamping process. Liu and Hua [8] fabricated metallic bipolar plate of SS304 stainless steel with micro-flow channels by using rubber pad forming process that are analyzed by the FEM using the commercial software ABAQUS. However, the main drawback of the rubber pad forming process is that the life of the rubber pad is not so long and should be replaced after the production of about 100 plates. Machining and cutting technologies for metallic bipolar plates are not used for mass production because of the high costs involved, even though these processes can provide the required high precision. In addition, metal forming processes (stamping and hydroforming), which can be used for mass production, have the forming limit problem.

On the other hand, high-pressure die casting (HPDC) is an ideal process for the fabrication of bipolar plates because it is a near-net-shape manufacturing process for arbitrary complicated shapes and mass production is possible with a high production rate. Niu et al. [9] reported that vacuum die casting reduces the gas porosity in the produced castings, which is caused by the entrapment of air in the molten metal. Therefore, its use could be applied to the manufacture of thin-walled parts. Despite the various advantages of HPDC, there has been little research on the fabrication of bipolar plates by die-casting processes because of the difficulty in manufacturing thin-walled parts with a thickness of less than 1 mm.

Computer-aided engineering (CAE) is one solution to this problem. Computational simulation offers a powerful and cost-effective way to study the effectiveness of various die designs through the analysis of filling and solidification behavior, so that improvements can be made in both product quality and process productivity, including the achievement of more effective control of the die filling and die thermal performance.

Solidification simulation (MAGMA soft) was carried out for the thin-walled die casting of aluminum (Al–Si–Cu alloy: ALDC12), with a thickness of 0.8 mm and the size of notebook computer housing. The results were used to fabricate thin-walled aluminum at the Korea Institute of Industrial Technology [10].

In this paper, the objective of this work is to present a feasibility study of the fabrication of thin-walled aluminum plate with a micro-flow channel by the vacuum die-casting process. In other words, this study aims to investigate the formability of bipolar plates for PEMFCs fabricated by vacuum die casting of an Al–Mg alloy (ALDC6) which has advantageous mechanical properties and superior corrosion resistance. The cavity of the mold consisted of a thin-walled plate shape (cavity size: 200 mm × 200 mm × 0.8 mm) with a layer of serpentine flow channel (active area: 50 mm × 50 mm).

Before the fabrication of bipolar plates by vacuum die casting, the filling behavior was simulated computationally using the MAGMA soft. The location and direction of the channel for the final mold design were determined by computational simulation. In addition, in order to investigate the relationship between injection speed and formability, simulations were conducted for different conditions of plunger stroke control (injection speed at low- and high-speed regions in sleeve), and the results were compared with those of actual die-casting experiments. The experimental results are then analyzed and discussed in terms of their formability, mechanical properties and microstructure of the formed bipolar plate.

2. Simulation and experimental process

2.1. Die design

The use of computational simulation for die design has many advantages over conventional methods involving the designer's experience or trial and error. In order to reduce the time and cost of the die design for a thin-walled aluminum plate with micro-channels, a commercial software package (MAGMA soft) was used in this study.

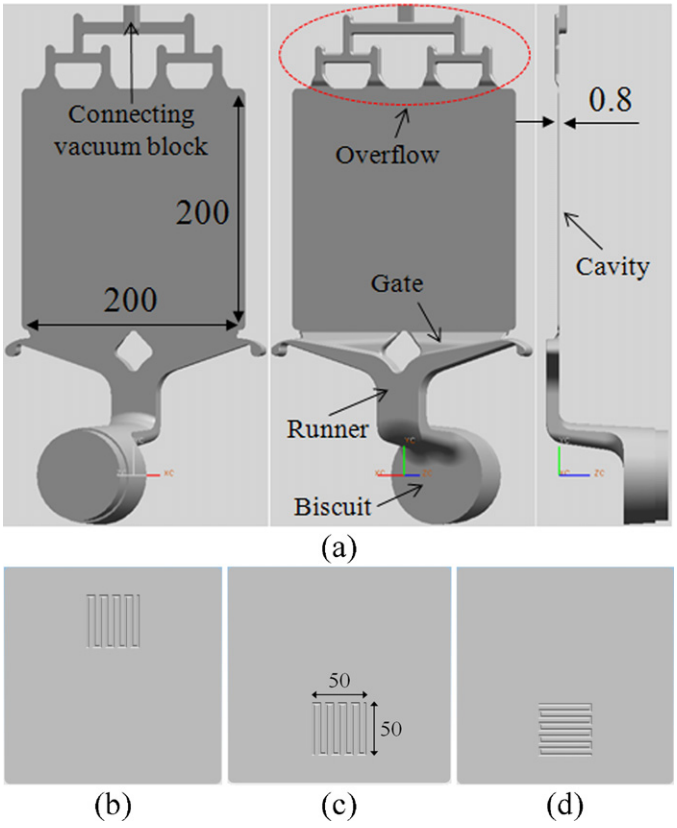

Fig. 1. Geometry of HPDC and type of die cavity model: (a) model 1, (b) model 2, (c) model 3 and (d) model 4 (unit: mm).

Because the design, location, and number of overflows are very important for obtaining good mechanical properties and superior formability, the die is designed with a total of four overflows in the final filling positions. Further, a vacuum vent is located at the end of the overflow to reduce gas porosity, which is caused by the entrapment of air or hydrogen gas in the molten metal during the high-speed injection of the molten metal into the cavity. Porosity is one of the major quality problems facing high pressure die casting. This is because porosity often causes leaking problems, surface defects and low mechanical properties.

The three-dimensional (3D) die modeling of the thin-walled plate and the type of die cavity model is used to determine the direction and location of the channel. The cavity size was 200 mm × 200 mm × 0.8 mm. Model 1 was a thin-walled plate containing a gating system, and overflow, model 2 was a thin-walled plate with a lengthwise (filling direction) channel near the overflow, model 3 was a thin-walled plate with a lengthwise channel near the gate, and model 4 was a thin-walled plate with a width wise channel near the gate, as shown in Fig. 1(a)–(d).

Park and Li [11] stated that the serpentine flow channel was widely chosen as flow channel designs for PEM fuel cells because it ensures the removal of water produced in a cell during the reactant flows along the flow channel, while with reasonable pressure drop, resulting in excellent cell performances. Boddu et al. [12] stated that for serpentine channels, the effective contact surface area of the gas channels can be increased by using square bends, because the square bends exhibit consistently lower pressure drops compared to curvilinear bends.

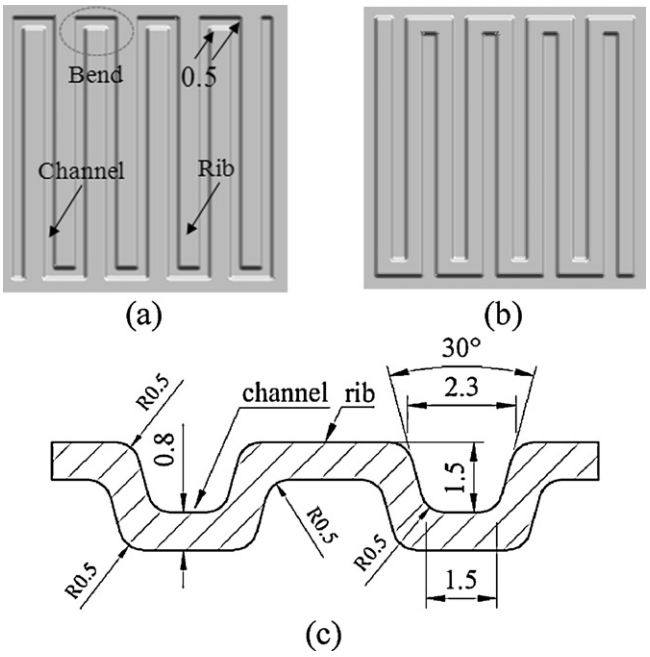

Fig. 2. Geometries of micro-channel: (a) top view, (b) bottom view and (c) section view (unit: mm).

The serpentine channel with square bends was therefore selected for channel design (Fig. 2). The active area of the bipolar plate is 50 mm × 50 mm. The width of the channel is 1.5 mm and channel depth of 1.5 mm is determined to investigate the effect of the maximum forming limit for them, and the numbers of gas channels, ribs, and square bends are 10, 11, and 8, respectively.

In addition, the width of the channel is designed to be set at radius of 0.5 mm and draft angle of 30° to facilitate removing the product from the die without tearing after injection and to ensure the fluidity of the molten metal passing through the channel.

2.2. Simulation conditions

The MAGMA soft package used in this study has the following characteristics:

(1) Ease of physical interpretation of various steps of algorithms.
(2) Conservation of physical properties.
(3) Better convergence than pure finite element or finite difference methods (FEM or FDM).
(4) Reduction of solution time.

The basic governing equations of the MAGMA soft software adopted for the filling and solidification analysis of the 3D incompressible fluid and control volume method are the continuity equation, Navier–Stokes equation, energy equation, volume of fluid (VOF), and governing finite differential equation (FDE) for the liquid-forming process.

For the thin-walled plate, the total numbers of meshes and metal cells in the Finite Volume Method (FVM) generated by mesh solver 5 in MAGMA soft were 7,313,242 and 241,126, respectively. For the thin-walled plate containing the channel, the total numbers of meshes and metal cells were 12,182,378 and 340,213, respectively.

The typical physical properties used for simulation in this study are listed in Table 1. The cast material for simulation was Al–Mg3 alloy in MAGMA data, the initial molten metal temperature was 720 °C, the die material was SKD61, and the die temperature was 200 °C. The general chemical composition of Al–Mg3 aluminum alloys is summarized in Table 2.

Table 1
Physical properties used in the high pressure die casting (HPDC) simulations.

Classification	Cast	Mold
Material	ALDC6	SKD61
Initial temperature of die, T_d	720 °C	200 °C
Liquidus temperature, T_{id}	645 °C	1458 °C
Solidus temperature, T_{sol}	595 °C	137 °C
Working pressure	50 kPa	
Diameter of plunger	75 mm	
Active length of shot sleeve	470 mm	
Shot sleeve filling	13.7%	
Area of the plunger	4417.865 mm^2	
Volume of shot sleeve	1546.253 cm^2	
Vacuum pressure	35 kPa	

Table 2
Chemical composition of Al–Mg3 aluminum alloys in MAGMA data (wt.%).

Mg	Si	Fe	Mn	Zn	Ni	Cu	Sn	Al
2.5–4.0	~1.0	~0.8	0.1–0.6	~0.4	~0.1	~0.1	~0.1	Bal.

Table 3
Heat transfer coefficients used in the HPDC simulations.

Classification	~T_{sol} (595 °C)	~T_{lid} (645 °C)
Cast/mold (h_{cd})	3000 W m^{-2} K^{-1}	7000 W m^{-2} K^{-1}
Mold/mold (h_d)	1000 W m^{-2} K^{-1}	

The heat-transfer coefficients used for simulation are shown in Table 3. In order to increase the effect of the heat transfer between the aluminum and the die, in this simulation, heat-transfer coefficients of 7000 and 3000 W m^{-2} K^{-1} for molten metal temperatures above the liquidus and below the solidus were used respectively. The value was 1000 W m^{-2} K^{-1} between dies, regardless of the molten metal temperature [13].

The die-casting machine used for the MAGMA soft simulations was a 660-ton cold-chamber die-casting machine, with a plunger diameter of 75 mm and a shot-sleeve active length of 470 nm. The switch over stages 1–2, the point at which the plunger moves from the low-speed to the high-speed region, was at 405 mm. The injection speed conditions are described in Table 4, and they were the same as those used in the actual die-casting experiments.

2.3. Experimental conditions

The concentration of hydrogen is one of the most important parameters for liquid aluminum because it is responsible for gas porosity, which affects casting quality. In order to obtain the optimum quality, the amount of hydrogen dissolved in the liquid aluminum must be known prior to die casting. Therefore, before

Table 4
Conditions of injection speed for plunger stroke control.

No	V_1 (m s^{-1})	V_2 (m s^{-1})
1	0.3	1.28
2	0.3	1.7
3	0.3	2.13
4	0.3	2.5
5	0.5	1.28
6	0.5	1.7
7	0.5	2.13
8	0.5	2.5
9	0.7	1.28
10	0.7	1.7
11	0.7	2.13
12	0.7	2.5

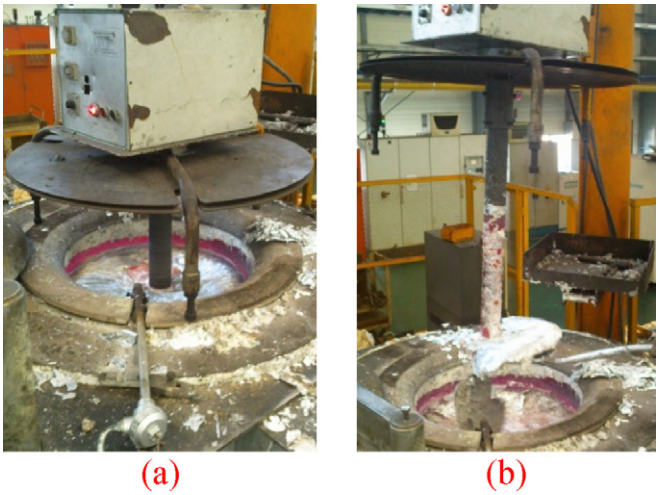

Fig. 3. The process of gas bubbling filtration: (a) during GBF and (b) impurities removal.

the die-casting test, a reduced-pressure test (RPT) was performed of the molten metal. The reduced-pressure test consists of solidifying a sample of the melt under reduced pressure (1–10 kPa range). This encourages pore formation, the pores expanding due to the lowered pressure than under atmospheric condition of solidification. The densitometer was used to compare the density of the sample solidified under vacuum with that of a sample solidified in a normal atmosphere. In the case where the density index was more than 1%, the gas-bubbling filtration (GBF) which reduces the amount of the hydrogen gas and inclusion in molten metal was carried out again. When the density index was less than 1%, the die-casting test was performed. The equation of density index is shown by the following expression:

$$\frac{(\rho_2 - \rho_1)}{\rho_2} \times 100(\%) \quad (1)$$

where ρ_2 is the density of sample in atmosphere, and ρ_1 is density of sample in vacuum. In this experiment, ρ_1 and ρ_2 are 2.659 g cm^{-3} and 2.679 g cm^{-3} respectively, density index therefore was about 0.75%. GBF process is shown in Fig. 3, the chemical composition of ALDC6 (Al–Mg alloy) as determined by component analysis is summarized in Table 5.

The 660-ton high-pressure die-casting machine with a vacuum system, moved die and fixed die is shown in Fig. 4. The vacuum system consisted of a vacuum pump, a vacuum tank, and a vacuum valve. The pouring temperature was controlled at 720 °C, and the die temperature was controlled at 200 °C oil using a heating unit during casting.

In the process of vacuum die casting (Fig. 5), V_1 is the plunger velocity in the low-speed region in the shot sleeve (where the molten metal reaches the gate), and V_2 is the plunger velocity in the high-speed region in the shot sleeve (where the molten metal moves from the gate to the overflow). After the molten metal was ladled into the pouring hole of the shot sleeve, the plunger moved to the end of the low-speed region (at 405 mm along the sleeve length) at a speed of V_1, and the vacuum pump was operated at a pressure of 35 kPa. From the low-speed region to the high-speed region, the plunger was moved to the end of the sleeve with a pressure of 50 MPa, and then the vacuum pump was deactivated. While the vacuum pump was working, a lower than atmospheric pressure was maintained in the die cavity, and the cavity was evacuated continuously from the beginning to the end of the die-filling process.

Table 5
Chemical composition of ALDC6 aluminum alloys after component analysis (wt.%).

Mg	Si	Fe	Mn	Ni	Cu	Sn	Zn	Al
2.420	0.620	0.470	0.420	0.074	0.071	0.040	0.030	*Bal*

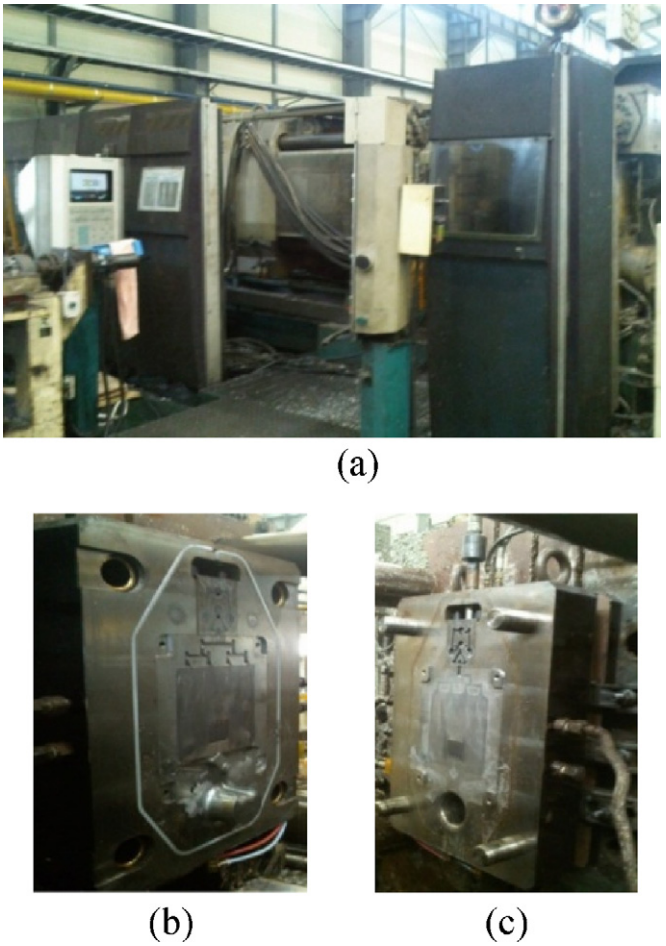

Fig. 4. (a) Vacuum die casting machine, (b) moved die and (c) fixed die.

The injection speeds of the low- and high-speed regions are detailed in Table 4; they are the same as those in the simulation. The injection test was conducted five times for each plunger speed. In order to investigate the effect of the vacuum, die casting was conducted five times without vacuum assistance under the best injection conditions for good formability. Then, solution treatment (at 520 °C for 5 h) was conducted to observe the blistering defects of the samples.

Fig. 6 schematically depicts the die-casting cavity divided into 12 parts used for the samples of hardness, thickness and microstructure. In order to investigate the effect of the injection speed at the channel part of the die-casting sample, two samples (7 and 8 of Position A) were made for hardness and microstructure analyses. Thickness, hardness, and microstructure analyses were also carried out for the sample prepared under the best injection conditions for formability. The hardness and microhardness of the samples were measured using a Vickers hardness tester (forces of 1 kg and 0.1 kg), thickness was measured by digital microscope and the microstructures were examined using an optical microscope (OLYMPUS BX 60M). X-ray analysis was conducted using a Toshiba Tosray-150 Hs Model. In addition, in order to measure the density of each sample fabricated under best injection conditions and no vacuum condition, the Archimedes principle was applied. The

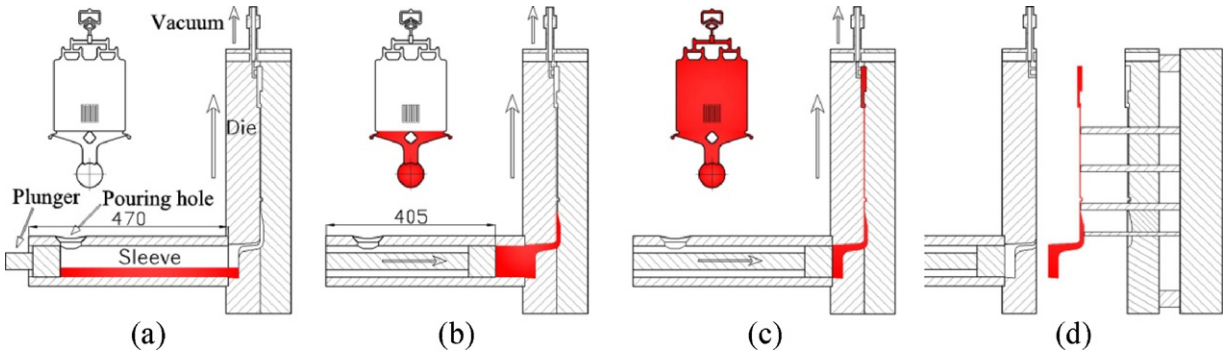

Fig. 5. Schematic diagram of the vacuum die casting process: (a) before move of plunger, (b) plunger moving at low speed region in sleeve (V_1), (c) plunger moving at high speed region in sleeve (V_2) and (d) romove product by ejector pin.

porosity fraction of each sample was calculated by the following equation:

$$f_p = \frac{(\rho_S - \rho_L)}{\rho_S} \times 100(\%) \quad (2)$$

where ρ_S is the standard density of an ALDC6 aluminum alloy (2.65 g cm^{-3}) and ρ_L is the measured density of sample by Archimedes principle.

3. Results and discussion

3.1. Simulation results for different cavity designs

The tangential-type gating system for forming a thin-walled plate of thickness 0.8 mm has no interference of each gate and ensures continuous melt flow during filling [10]. The prediction of the filling behavior of the melt is important for the die design for bipolar plates. When the melt flowed on the die cavity past the gate, the filling behavior and temperature distribution of the melt in the channel part of the die cavity were investigated for each cavity shape model.

The temperature distribution found with the four types of cavity is presented in Fig. 7 (under injection speed condition 2). As shown in Fig. 7(a), the flow of the melt was divided into three at the 90% filling state, but the flow became unified again due to the continuous entry of the melt. The temperature of the melt dropped near the overflow. It was found that superior flow could be achieved with the tangential-type gating system by changing the injection speed. As shown in Fig. 7(b) (model 2), this is expected to cause misrun and casting defects because the temperature drop of the melt occurs at the channel part. As shown in Fig. 7(c) (model 3), although the flow of the melt was slightly spattered at the end of the channel part, uniform temperature distribution and filling behavior were observed. As shown in Fig. 7(d) (model 4), the flow of the melt was severely broken and the temperature drop occurred at the channel part because the melt flowed along the channel width (1.5 mm) and several ribs. This is also expected to cause misrun and many casting defects.

On the basis of the simulation results, model 3 was selected as the die cavity design because the melt flowed uniformly in the die cavity and the temperature drop occurred only near the overflow.

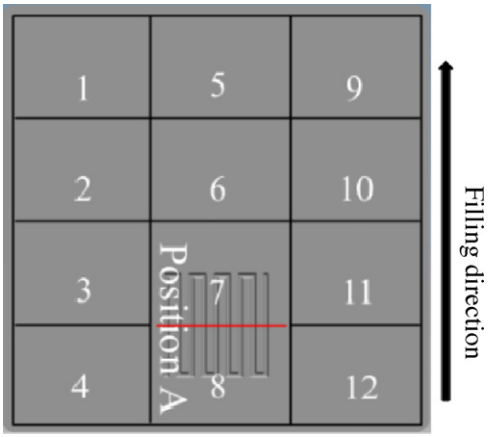

Fig. 6. The schematic illustration of 12 samples in die casting cavity.

3.2. Experimental and simulation results for different injection speeds

Experiments and computational simulations were carried out for different injection speeds. The range of possible forms using various injection speeds (as in Table 4) obtained from the experimental

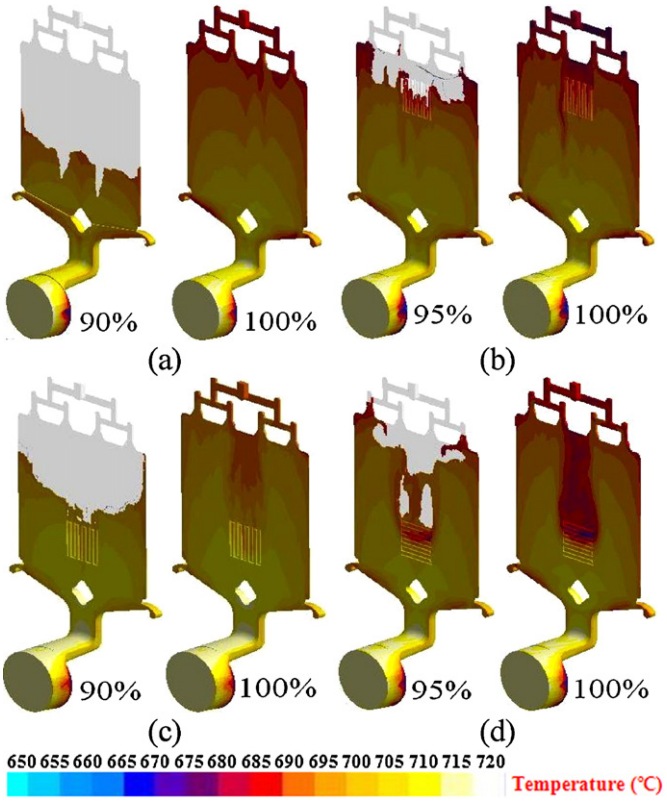

Fig. 7. Temperature distribution for each model (under injection speed condition 2): (a) model 1, (b) model 2, (c) model 3 and (d) model 4.

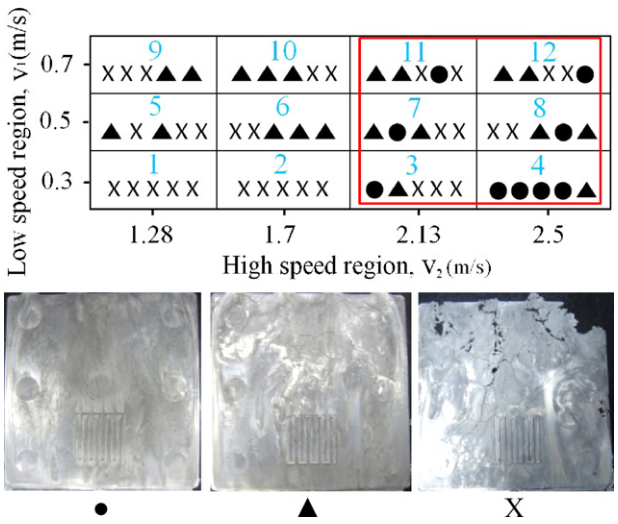

Fig. 8. Experiment result for different conditions of injection speed (●: perfect and ▲ defects; X: misrun).

results of actual vacuum die casting is shown in Fig. 8. The symbol "●" signifies a perfectly filled sample without casting defects, and "▲" shows that the sample had casting defects from the end of the channel to the overflow, even though the sample was nearly filled. The "X" symbol denotes misrun.

Based on the results shown in Fig. 8, misrun occurred mainly when the injection speed was low in the low- and high-speed regions. In particular, when the injection speed of the low-speed region was above 0.3 m s^{-1}, it had no influence on the formability, and when the injection speed in the high-speed region was above 2.13 m s^{-1}, good samples were obtained. In other words, the higher the injection speed of the high-speed region, the more effective the formability. The best injection speeds are 0.3 and 2.5 m s^{-1} in the low- and high-speed regions, respectively (condition 4), and it gave rise to a sample more than 80% perfect. However, most conditions caused misrun, probably owing to the shortage of silicone (which is related to castability) in ALDC6 and the low fluidity of the melt flowing along the channel width (1.5 mm) and several ribs.

These results indicate that more overflows should be added to the final filling position to eliminate the premature freezing of the melt. Also, in the case of thin-walled die casting, the melt needs to have laminar flow, which can be achieved by setting a low injection speed in the low-speed region because of the thin gate and cavity. A high injection speed should be set in the high-speed region to prevent premature solidification of the melt in the final filling position.

The simulation (filling temperature, velocity, air-entrapment) and actual vacuum die-casting results are presented in Fig. 9. As shown in Fig. 9(a)–(d), the velocity was 20 m s^{-1} at the runner and gate, and it dramatically increased to more than 40 m s^{-1} at the entrance to the cavity because the melt passed through a thin gate when the plunger was moved rapidly in the high-speed region. In addition, it is seen that the velocity increased sharply to 100 m s^{-1} adjacent to the overflow because of the narrow overflow entrance.

For conditions 1 and 4 in Table 4, the final filling times (from Fig. 5(a)–(c)) in the die cavity were 1.373 and 1.365 s, respectively. For conditions 9 and 12 in Table 4, the final filling times in the cavity were 0.6 and 0.592 s, respectively. Therefore, the final filling time was affected more by the velocity of the low-speed region than by that of the high-speed region.

As shown in Fig. 9(a) and (b), because the velocity at the entrance of the cavity was low (about 40 m s^{-1}) and the temperature (about 685 °C) and velocity (about 25 m s^{-1}) decreased as a result of the

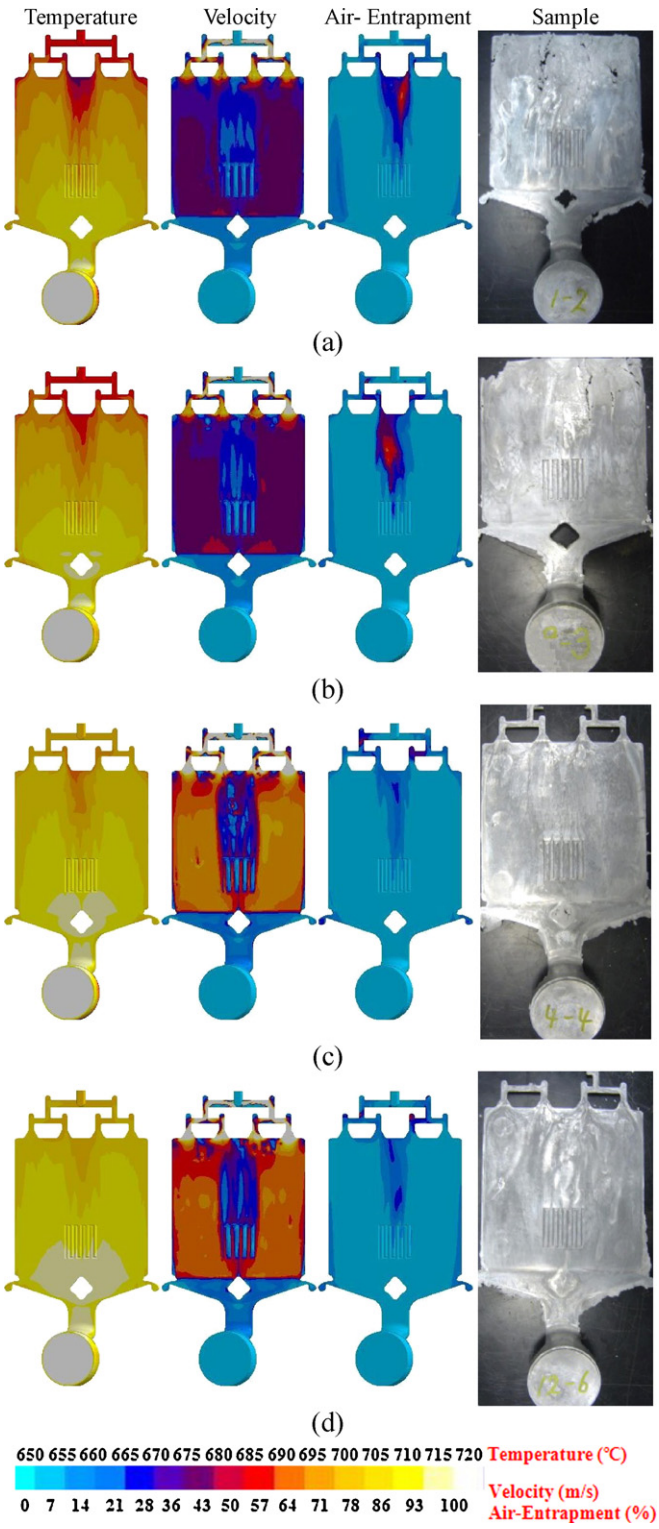

Fig. 9. Simulation results (filling temperature, velocity, air-entrapment) and samples for injection speed conditions: (a) condition 1, (b) conditon 9, (c) conditon 4 and (d) conditon 12.

low velocity in the high-speed region, the melt was partially cooled from the end of the channel and the trapped air or gas (mostly hydrogen) dissolved in the melt was not eliminated by the vacuum vent. As a result, it was seen that the sample had many casting defects in the cavity, such as misrun, cracks and flow marks. On the other hand, as shown in Fig. 9(c) and (d), when the velocity at the entrance of the cavity was 60 m s^{-1} and the temperature

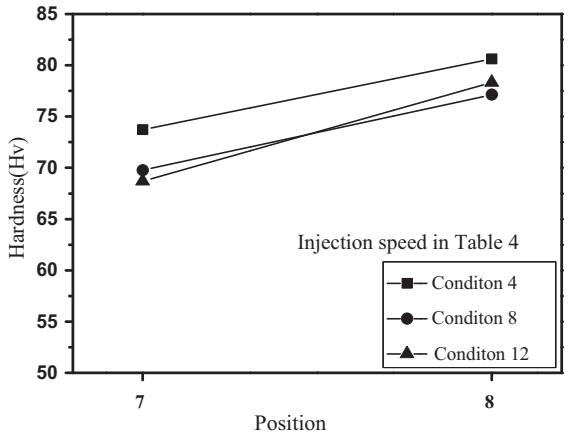

Fig. 10. Hardness of samples at position A (7 and 8) for injection conditions 4, 8 and 12.

and velocity drop decreased from the channel part due to the high velocity in the high-speed region, a uniform temperature distribution was secured and the trapped air or gas was nearly eliminated by the vacuum vent. The sample obtained under condition 4 had few casting defects except for some flow marks adjacent to the overflow (Fig. 9(c)), and that obtained under condition 12 had a few casting defects including flow marks and small cracks caused by solidification contraction (Fig. 9(d)).

On the basis of the experimental and simulation results, injection condition 4 (V_1: 0.3 m s^{-1}; V_2: 2.5 m s^{-1}) is the best condition for fabrication of bipolar plates.

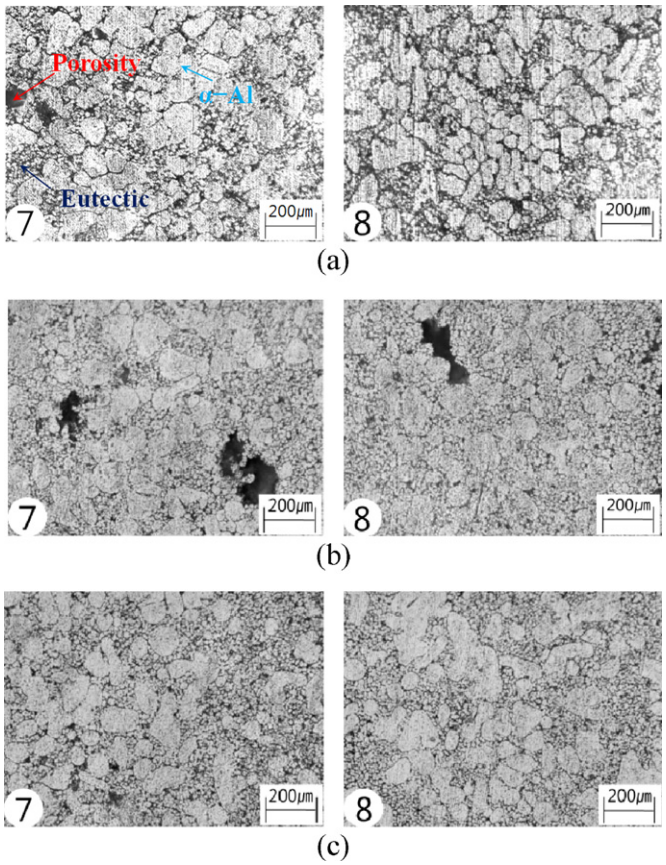

Fig. 11. Microstructures of samples at position A (7 and 8) for injection speed conditions: (a) condition 4, (b) condition 8 and (c) condition 12.

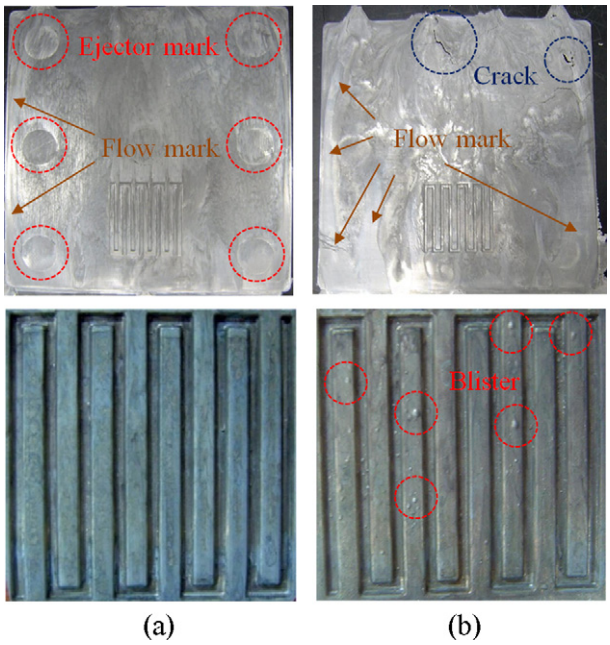

Fig. 12. Comparison of sample surface defects and blister of channel part: (a) between vacuum die casting and (b) conventional die casting.

3.3. Analysis of experimental results

3.3.1. Effect of injection speed on hardness and microstructure

The relationship between the hardness and position A (shown in Fig. 6) of the samples fabricated under conditions 4, 8, and 12; these conditions led to samples with superior formability being obtained is shown in Fig. 10. The relationship between the microstructure and position A is shown in Fig. 11.

The hardness test samples were used for all micrographs, so the positions of microscopic observation were the same as those used for hardness testing (Fig. 6).

The phases present in the microstructure are largely primary α-Al and eutectic mixtures (all zones except for α-Al). The α-Al phase is a solid solution rich in aluminum, while the eutectic mixture is composed of fine α-Al phases, Mg phases, and others. Also, the dark and coarse parts of the microstructure indicate porosity. Because aluminum is soft compared to magnesium, the α-Al phase is accordingly softer than the eutectic mixture. The Vickers microhardness of the α-Al phase is about 60 Hv, while that of the eutectic mixture is in the range of 70–85 Hv.

After the Vickers hardness of the sample was measured five times, the average hardness was calculated (excluding the maximum and minimum values). As shown in Fig. 9, the hardness of the sample fabricated under condition 4 was higher than those of the samples made under conditions 8 and 12 at all locations of position A. The hardness of position 7 is lower than that of positions 8. This result arises from the fact that the samples prepared under conditions 8 and 12 had high porosities. Porosity fraction of condition 4

Table 6
Density and porosity fraction of each sample for injection speed conditions (No vacuum: condition 4 without vacuum assistance).

Condition	Density (g cm^{-3})	Porosity fraction (%)
4	2.6150	1.32
8	2.5860	2.42
12	2.5934	2.13
No vacuum	2.4765	6.54

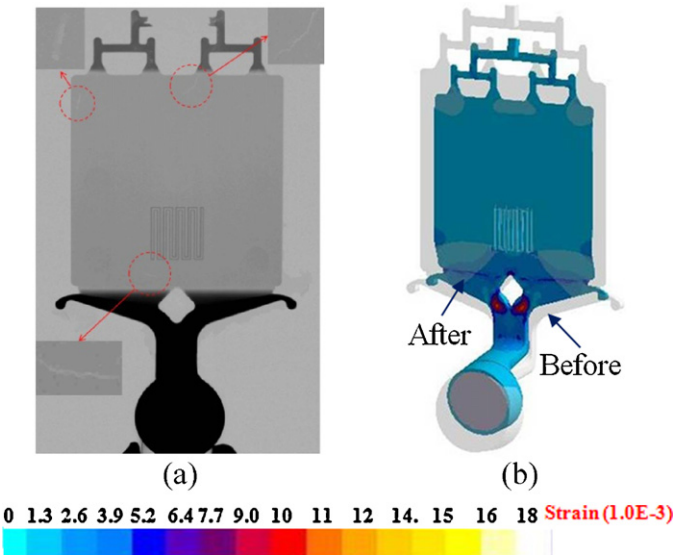

Fig. 13. Result of (a) X-ray analysis and (b) solidification contraction.

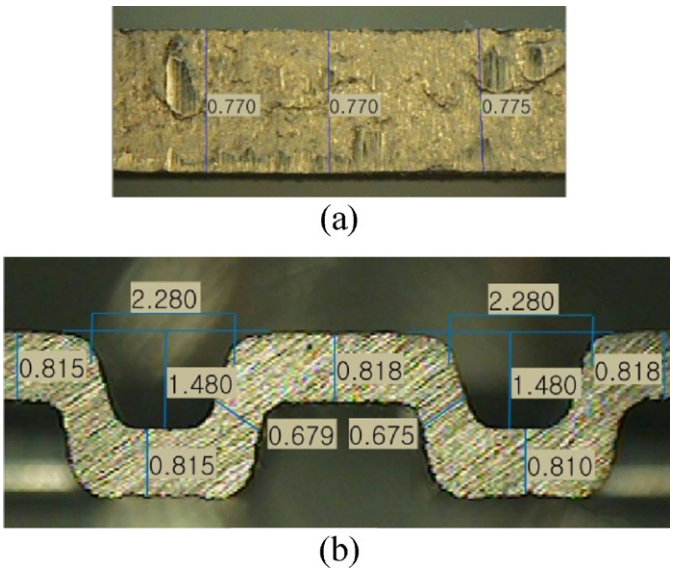

Fig. 14. Thickness measurement of sample by digital microscope: (a) plate part and (b) channel part.

(1.32%) is lower than that of condition 8 (2.42%) and 12 (2.13%) as shown in Table 6.

The reason for this may be explained as follows. When the molten metal flows in the channel, it is partially solidified before the whole volume of melt is injected into the die cavity. This premature solidification of the melt causes an obstacle and makes it impossible for the remaining volume of melt to be injected into the overflow. The porosity is therefore caused by the premature solidification of the melt and the entrapment of air or gas, and as a result, high hardness is not achievable.

3.3.2. *Effect of vacuum assistance on formability and surface defect*

In order to investigate the effect of the vacuum, die-casting experiments five times without vacuum assistance under condition 4 were conducted, and then solution treatment at 520 °C for 5 h carried out to observe the amount of porosity in the samples, which were first cut in the channel part. The surface defect observed was blistering defects. The results showed that misrun had occurred in three samples, and the other two had cracks caused by solidification contraction and flow marks from the end of the channel as

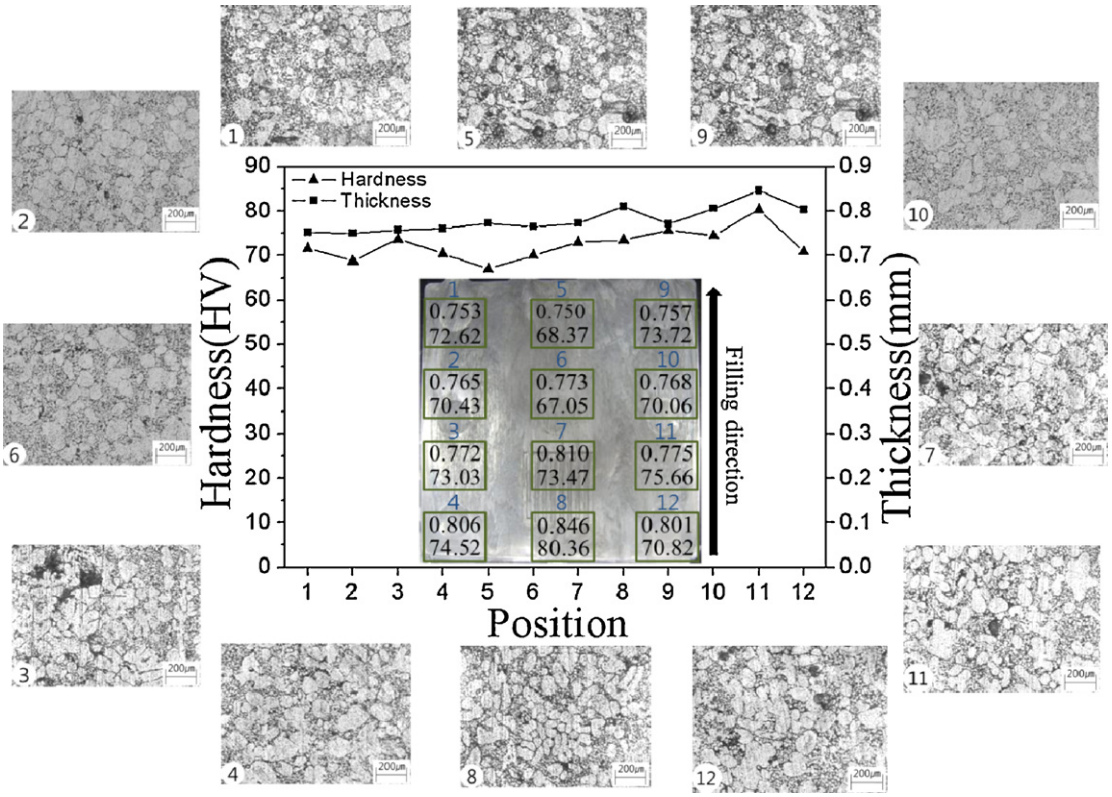

Fig. 15. Thickness, hardness and microstructures of sample at different positions.

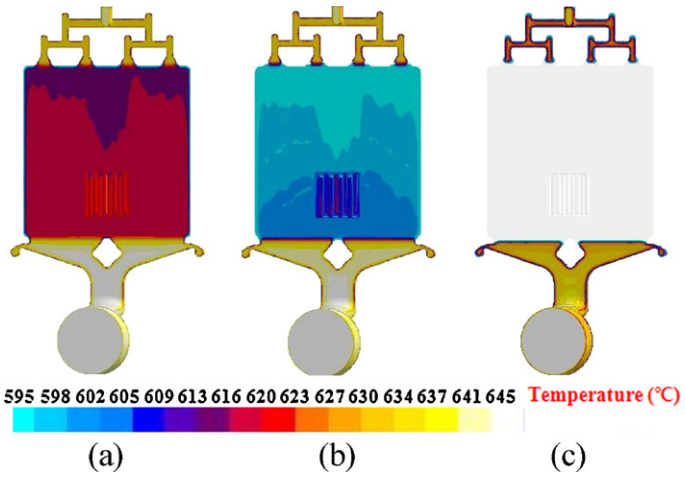

Fig. 16. Simulation results of solidification behavior: (a) 13% state, (b) 15% state and (c) 20% state.

shown in Fig. 12(b), top. Blistering defects are mostly seen in the case of channel sample manufactured by conventional die casting (porosity fraction: 1.32%). On the other hand, the channel samples fabricated by vacuum die casting has few blisters (porosity fraction: 6.54%) in Fig. 12, bottom.

These results indicate that in case of thin-walled plates, vacuum die casting is beneficial in terms of formability compared to conventional die casting, and the vacuum assistance also has a distinct advantage in terms of the reduced porosity of the samples.

3.3.3. X-ray analysis of sample

In order to observe defects that are invisible to the naked eye inside the sample fabricated under condition 4, X-ray experiments were conducted (Fig. 13(a)). Cracks can be observed around the overflow and gate. As shown in the simulation results (Fig. 13(b)), the cracks occur in the high solidification contraction parts of the cavity connected to the gate and overflow. The high solidification contraction is caused by the fact that the thicknesses of the gate and overflow are different from that of the cavity.

3.3.4. Thickness, hardness and microstructure by sample position

The sample fabricated under condition 4 was cut to twelve samples for metallographic examination, hardness and thickness measurement. The thickness, hardness and microstructure of the sample at different positions (as noted in Fig. 6) are shown in Figs. 14 and 15 respectively. The average thickness and hardness of the samples were 0.78 mm and 70.37 Hv, respectively. The thickness of the sample adjacent to the gate was more than 0.8 mm; this decreased to less than 0.8 mm as it approached the overflow. Likewise, the hardness of the sample adjacent to the gate was higher than the average, and it decreased to less than 70 Hv upon approaching the overflow. This result is probably due to solidification contraction and defects such as flow marks, ejector mark and porosity in microstructure.

The remarkable differences between the microstructures are the size of the α-Al phases and the amount of the porosity. Porosity can be observed all over the micrographs, but it increased adjacent to the overflow (1, 5, and 9). A coarse α-Al phase with similar dendritic shape was observed adjacent to the gate (first-filled position). In contrast, a fine α-Al phase was observed adjacent to the overflow (last-filled position). Also, eutectic mixtures were commonly observed in the last-filled positions. It is considered that because the sample thickness of the last-filled position is thin compared with the first-filled position, the solidification speed of the last-filled position is faster than that of the first-filled position (Fig. 16). Therefore, fine α-Al phases and many eutectic phases are present in the microstructure of the last-filled positions, as shown in Fig. 15.

4. Conclusions

For the fabrication of aluminum bipolar plates using vacuum die casting of ALDC6, the formability, mechanical properties, and microstructure results according to die design and injection speed can be summarized as follows:

(1) Model 3 is suitable for die design for a bipolar plate with a lengthwise channel near the gate.
(2) Injection condition 4 (V_1: 0.3 m s^{-1}; V_2: 2.5 m s^{-1}) is the best condition for fabrication of bipolar plates. The higher the injection speed of the high-speed region, the more effective the formability.
(3) Because porosity fraction of condition 4 is lower than that of condition 8 (V_1: 0.5 m s^{-1}; V_2: 2.5 m s^{-1}) and 12 (V_1: 0.7 m s^{-1}; V_2: 2.5 m s^{-1}), the hardness of condition 4 was higher than those of the conditions 8 and 12.
(4) Vacuum die casting is more beneficial than conventional die casting in terms of the formability and porosity removal of the sample.
(5) More over flows should be added to the final filling position to eliminate prematurely freezing melt.

Acknowledgments

This work was supported by the National Research Foundation of Korea (NRF) grant founded by the Korea Government (MEST) (NO. 2009-0081077). This work was also supported by the human resources development of the Korea Institute of Energy Technology Evaluation and Planning (KETEP) grant funded by the Korea government, Ministry of Knowledge Economy (No. 20104010100540).

References

[1] E. Middelman, W. Kout, B. Vogelaar, J. Lenssen, E. de Wall, J. Power Sources 118 (2003) 44–46.
[2] T. Matsuura, M. Kato, M. Hori, J. Power Sources 161 (2006) 74–78.
[3] A. Hermann, T. Chaudhuri, P. Spagnol, Int. J. Hydrogen Energy 25 (2000) 1297–1302.
[4] H. Tawflk, Y. Hung, D. Mahajan, J. Power Sources 163 (2007) 755–767.
[5] S.J. Lee, C.Y. Lee, K.-T. Yang, F.-H. Kuan, P.H. Lai, J. Power Sources 185 (2008) 1115–1121.
[6] J.C. Hung, T.-C. Yang, K.-C. Li, J. Power Sources 196 (2011) 2070–2074.
[7] S. Mahabunphachai, O.N. Cora, M. Koc, J. Power Sources 195 (2010) 5269–5277.
[8] Y. Liu, L. Hua, J. Power Sources 195 (2010) 3529–3535.
[9] X.P. Niu, B.H. Hu, I. Pinwill, I. Li, J. Mater. Process. Technol. 105 (2000) 119–127.
[10] Y.C. Kim, C.S. Kang, J.I. Cho, C.Y. Jeong, S.W. Choi, S.K. Hong, J. Mater. Sci. Technol. 24 (2008) 383–388.
[11] J. Park, X. Li, J. Power Sources 163 (2007) 853–863.
[12] R. Boddu, U.K. Marupakula, B. Summers, P. Majumdar, J. Power Sources 189 (2009) 1083–1092.
[13] D.H. Lee, C.G. Kang, P.K. Se0, J. Mater. Process. Technol. 147 (2004) 45–50.